# Defect physics of $CuGaS_2$

Christine L. Bailey,[1] Leandro Liborio,[2] Giuseppe Mallia,[2] Stanko Tomić,[1] and Nicholas M. Harrison[1,2]
[1]*Computational Science and Engineering Department, STFC Daresbury Laboratory, Daresbury, Warrington, Cheshire WA4 4AD, United Kingdom*
[2]*Thomas Young Centre, Department of Chemistry, Imperial College London, Exhibition Road, London SW7 2AZ, United Kingdom*
(Received 18 March 2010; revised manuscript received 28 April 2010; published 28 May 2010)

Hybrid density-functional theory has been used to study phase stability and defect formation in the $CuGaS_2$ chalcopyrite. The equilibrium population of intrinsic defects is predicted and it is shown that the material is intrinsically *p*-type doped. Extrinsic defects consisting of elements from group II, group IV, and group VII of the periodic table are studied. It is predicted that *n*-type doping of $CuGaS_2$ is not possible through the addition of these extrinsic defects. The stability of the ordered defect compounds $CuGa_3S_5$ and $CuGa_5S_8$ is also investigated. These compounds are shown to be stable only in a very narrow region of phase space.

DOI: 10.1103/PhysRevB.81.205214 PACS number(s): 71.15.Mb, 71.20.Nr, 71.55.Ht

## I. INTRODUCTION

$CuGaS_2$ is a member of the Cu-III-$VI_2$ chalcopyrite family and has a direct band gap of 2.43 eV at the Γ point. This is a significantly larger band gap than those observed in the chalcopyrites $CuGaSe_2$, $CuInSe_2$, and $CuInS_2$, which are used in single-junction solar cells. There is, however, much interest in the use of $CuGaS_2$ in third-generation solar cells. While single-junction devices are limited to a solar conversion efficiency of 31% under one sun illumination,[1] efficiencies of 30–60 % are being targeted by third-generation devices. Technologies including intermediate band (IB) and multijunction cells are being used to obtain these high efficiencies.

Introducing an IB into the band gap of a solar cell enables multiple photon transitions.[2,3] Photons can be excited from the valence band (VB) to the IB, from the IB to the conduction band (CB) and also directly from the VB to the CB. This increases the overall efficiency of the device compared to a single-junction solar cell. The theoretical limit on the efficiency of an IB solar cell is 47% under one sun illumination.[4] The ideal host material would have a band gap of 2.41 eV with an IB located at 0.92 eV from either the CB or the VB.[4] $CuGaS_2$ is, therefore, a promising host material for such a device. Theoretical studies suggest that doping this material with the transition metals Ti or Cr may lead to isolated IBs.[5,6]

Multijunction solar cells consist of two or more layers of absorbers, each with a different band gap, enabling light to be collected at multiple wavelengths. A promising material for such a device is $Cu(In,Ga)(S,Se)_2$ (CIGSSe). Recent spectroscopy data suggests a depth dependence of the band gap within CIGSSe.[7] This may enable photon absorption at different wavelengths, without the difficult and expensive requirement to grow several pseudomorphically mismatched layers. The depth-dependent variation of the band gap in CIGSSe is attributed to a depth dependency of S concentration. Regions that are rich in S exhibit larger band gaps compared to those that are poor in S.

A suitable band gap is by no means the only criteria for an efficient solar cell. An additional requirement is that the material can be type inverted, as this leads to band bending at the interface between the absorber and the buffer layer (e.g., CdS). Thin-film solar cells based on $CuInSe_2$ are highly efficient, in part because, while the bulk $CuInSe_2$ material is *p* type, its surface can be type inverted to become *n* type.[8,9]

In this study, $CuGaS_2$ is characterized using hybrid exchange density-functional theory (DFT). Full details of the methodologies used are given in Sec. II. The calculated geometric and electronic structure of bulk $CuGaS_2$ are discussed in Sec. III A. In Sec. III B, the relative stability of $CuGaS_2$ with respect to other competing phases is studied. The formation of intrinsic defects is investigated in Sec. III C; defects consisting of Cu, Ga, and S vacancies ($V_{Cu}, V_{Ga}, V_S$), Ga substitution of Cu atoms ($Ga_{Cu}$) and vice versa ($Cu_{Ga}$) are modeled. Neutral and charged defects are considered, for example, vacancies formed by removal of both a neutral Cu atom ($V_{Cu}$) and a $Cu^+$ ion ($V_{Cu}^-$). The carrier concentration of $CuGaS_2$ is calculated as a function of the formation energies of these intrinsic defects and it is shown that the material is always intrinsically *p*-type doped.

It has previously been shown that compound defects consisting of two $V_{Cu}^-$ defects and a $Ga_{Cu}^{2+}$ (or $In_{Cu}^{2+}$) defect are energetically favorable compared to the three isolated defects in the $CuGaSe_2$ and $CuInSe_2$ chalcopyrites.[10,11] The ordering of these compound defects leads to the formation of phases such as $CuGa_3Se_5$ and $CuGa_5Se_8$. In Sec. III D, the formation of $2V_{Cu}^- + Ga_{Cu}^{2+}$ compound defects in $CuGaS_2$ is studied and the structure and thermodynamics of $CuGa_3S_5$ and $CuGa_5S_8$ are computed.

Extrinsic defects such as group VII elements of the periodic table (Cl, Br, and I) substituting S ($VII_S$) or group IV elements (Ge and Sn) substituting Ga ($IV_{Ga}$) might be expected to lead to *n*-type doping of $CuGaS_2$. The addition of group II elements (Mg, Zn, and Cd) may also *n*-type dope the material if they preferentially replace Cu ($II_{Cu}$) rather than Ga ($II_{Ga}$). In Sec. III E, the free energy of formation of these extrinsic defects is discussed and it is predicted that, although thermodynamically stable, they do not lead to overall *n*-type doping of the material. Finally, in Sec. IV, the main conclusions of this study are summarized.

 

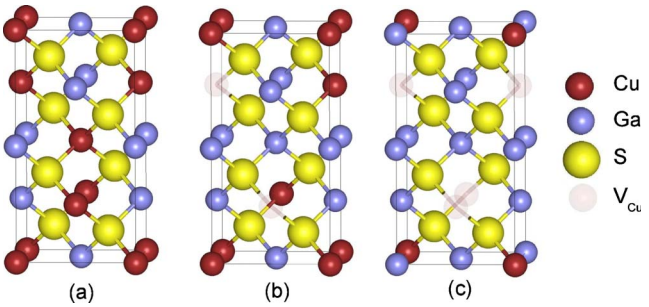


FIG. 1. (Color online) The crystal structures of (a) $CuGaS_2$; (b) $2V_{Cu}^{-}+Ga_{Cu}^{2+}$ in $CuGaS_2$; (c) $CuGa_5S_8$. The (16 atom) conventional unit cell of $CuGaS_2$ is shown. The $2V_{Cu}^{-}+Ga_{Cu}^{2+}$ compound defect and $CuGa_5S_8$ are calculated in $(2\times2\times1)$ supercells. There are alternating rows of Ga-Cu-Ga-Cu atoms along the *a* and *b* axes of $CuGa_5S_8$.

## II. METHODOLOGY

### A. Computational details

Theoretical results presented in this paper are based on DFT calculations performed using CRYSTAL (Ref. 12) and the B3LYP hybrid exchange functional.[13] This functional has been shown to provide a reliable description of geometric and electronic structure and energetics in a wide range of materials.[14,15] In particular, hybrid exchange functionals, such as B3LYP, provide a much better prediction of the band gap of semiconductors than local-density or generalized gradient approximations. In CRYSTAL, the convergence of the real-space summation of the Coulomb and exchange contributions to the Hamiltonian matrix is controlled by five overlap criteria. The values used in this study were $10^{-6}$, $10^{-6}$, $10^{-6}$, $10^{-6}$, and $10^{-12}$. The control of these approximations is described in detail elsewhere.[12] A Monkhorst-Pack shrinking factor of 6 was used to sample the first Brillouin zone and a denser Gilat net consisting of 12 points was used in the evaluation of the Fermi energy and density matrix.[12] Polarized triple-valence Gaussian basis sets were used throughout. In the case of Ga, a pseudopotential was used to describe the core electrons.[16] The basis sets have been used in previous studies[15–19] and are listed in the supplementary material.[20] Defect formation energies consisting of S anion vacancies were calculated by removing the S atom while retaining its associated basis functions to describe the possible localization of electrons within the vacancy (see Sec. II F). For the calculation of Cu and Ga cation vacancies, the atom and its associated basis functions were removed as these vacancies do not donate electrons to the system.

### B. Crystal structures

$CuGaS_2$ adopts the $I\bar{4}2d$ space group. Each S anion is tetrahedrally coordinated to two Cu cations and two Ga cations, as shown in Fig. 1(a). The S anion adopts an equilibrium position that is closer to one type of cation than the other. The anion displacement, *u*, measures the extent of the unequal bond lengths in the system; it is given by

TABLE I. The change in the energy of a neutral $CuGaS_2$ system when an electron is removed.

| No. of atoms | $E_{DFT}(CuGaS_2)-E_{DFT}(V^+)$ (eV) |
|---|---|
| 8 | 6.834 |
| 32 | 6.993 |
| 64 | 7.090 |
| 128 | 7.115 |
| 256 | 7.133 |
| 512 | 7.143 |

$$u = 0.25 + (R_{CuS}^2 - R_{GaS}^2)/a^2, \tag{1}$$

where $R_{CuS}$ and $R_{GaS}$ are the Cu-S and Ga-S bond lengths, respectively, and *a* is a lattice parameter. Defects were modeled in 64-atom supercells obtained by doubling the *a* and *b* axes of the $CuGaS_2$ conventional cell, and referred to here as a $(2\times2\times1)$ supercell. The compound defect $2V_{Cu}^{-}+Ga_{Cu}^{2+}$ is shown in Fig. 1(b). $CuGa_5S_8$, was modeled within a $(2\times2\times1)$ supercell, part of which is shown in Fig. 1(c). $CuGa_3S_5$ was modeled within a $(1\times1\times5)$ supercell.[10]

### C. Energy corrections for charged defects

A consequence of using periodic boundary conditions within electronic structure calculations is that the boundary conditions lead to the conditional convergence of the Coulomb potential. In the case of uncharged systems, the potential and total energy converge to well-defined values under the conditions described first by Ewald.[21] The total energy of a charged system, however, can only be calculated to within a constant offset value.[22] The value of this offset depends on the average crystal potential. It can be obtained by calculating the change in the energy of a neutral system when an electron is removed from it for increasing system size. As the system size increases, this change in energy will converge to the value of the offset. The resultant energy differences for the $CuGaS_2$ system before and after the removal of an electron are given in Table I. In this paper, the total energy of charged cells include the addition of a constant offset of 7.15 eV multiplied by the net charge of the system.

In addition to the constant offset, a second correction is also necessary. The calculation of charged defects requires the addition of a uniform background charge to neutralize the cell, as the total energy would diverge for a periodically repeating charged system. The total energy of a periodic system consisting of a localized charged defect includes terms due to defect-defect, defect-background, and background-background Coulomb interactions. The calculation of these terms is necessary for an accurate determination of the energy of an isolated defect and can be approximated by the multipole correction,[23]

$$\Delta E = \frac{q^2\alpha_M}{2\epsilon_r V^{1/3}} + \frac{2\pi qQ}{3\epsilon_r V} + O(V^{-5/3}), \tag{2}$$

where $\alpha_M$ is the lattice-dependent Madelung constant and *V* is the volume of the cell. $\epsilon_r$ is the static relative dielectric

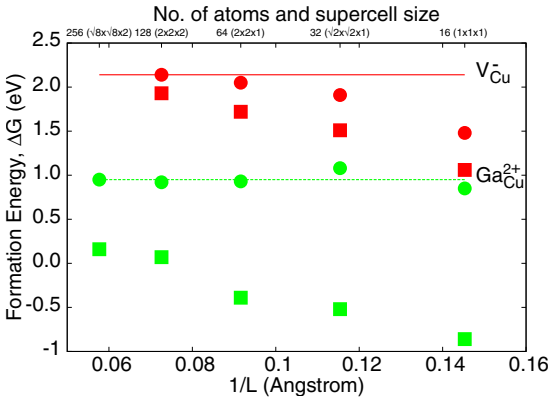


FIG. 2. (Color online) The formation energies of $V_{Cu}^{-}$ and $Ga_{Cu}^{2+}$ defects in $CuGaS_2$. The squares and circles, respectively, denote calculated formation energies before and after first-order corrections [given by Eq. (2)] are applied.

constant, measured in units of the vacuum dielectric constant, $\epsilon_0$. The calculated value of $\epsilon_r$ for $CuGaS_2$, using the finite-field perturbation method,[24] is $5.7\epsilon_0$ (compared to an observed value of $5.8\epsilon_0$). $Q$ is the quadrupole moment of the defect.

The formation energy of $V_{Cu}^{-}$ and $Ga_{Cu}^{2+}$ defects as a function of increasing supercell sizes has been calculated. To isolate the purely electrostatic effects these calculations were performed without any geometry optimization. The resultant energies before and after first-order corrections [first term in Eq. (2)] are shown in Fig. 2. The horizontal lines in this figure represent the calculated energies for the largest supercell sizes. The convergence of the formation energies cannot be significantly improved through the addition of a second-order correction term. It is, however, possible to improve the convergence of the $V_{Cu}^{-}$ defect energies by increasing the prefactor of the $1/V^{1/3}$ term. This may be partially compensating for additional factors, such as elastic screening.[25] While, in principle, it would be possible to analyze the rate of convergence of a fully relaxed supercell for each defect considered in this study, it would be prohibitively computationally expensive to do so. Analysis of these results suggests that defect formation energies can be calculated to within an accuracy of 0.2 eV for a 64-atom supercell after including first-order corrections given by Eq. (2). All subsequent defect formation energies in this paper are calculated at this level of precision.

### D. Phase stability

The Gibbs free energy ($G$) and Gibbs free energy of formation ($\Delta G$) of a charge-neutral incompressible solid, with respect to its constituent elements, $i$, are given by

$$G = \sum_i n_i \mu_i, \tag{3}$$

$$\Delta G = \sum_i n_i \Delta \mu_i, \tag{4}$$

where $n_i$ is the total number of atoms of element $i$ in the system and $\Delta\mu_i = \mu_i - \mu_i^\circ$, where $\mu_i$ is the absolute value of the chemical potential and $\mu_i^\circ$ is the chemical potential of element $i$ in its standard state. The allowed values of $\Delta\mu_i$ are determined from a set of thermodynamic limits. The upper bound is $\Delta\mu_i \leq 0$ as at this point precipitation of element $i$ to its standard state occurs.

In the region of phase space in which $CuGaS_2$ is stable, the chemical potentials of the constituent atoms must equal the Gibbs free energy of formation of $CuGaS_2$,

$$\Delta G_{CuGaS_2} = \Delta\mu_{Cu} + \Delta\mu_{Ga} + 2\Delta\mu_S. \tag{5}$$

The chemical potentials are further constrained by the formation of competing phases, such as $Cu_2S$ and $Ga_2S_3$,

$$2\Delta\mu_{Cu} + \Delta\mu_S \leq \Delta G_{Cu_2S}, \tag{6}$$

$$2\Delta\mu_{Ga} + 3\Delta\mu_S \leq \Delta G_{Ga_2S_3}. \tag{7}$$

Other competing binary phases (CuS and GaS) were also considered.

The Gibbs free energy is also given by $G = U + pV - TS$, where $U$ is the internal energy, $p$ is the pressure, $V$ is the volume, $T$ is the temperature, and $S$ is the entropy of the system. The $pV$ and $TS$ terms are small for highly incompressible materials such as $CuGaS_2$, furthermore, in the following equation they approximately cancel one another,[26,27]

$$\Delta G_{CuGaS_2} \approx E_{DFT}(CuGaS_2) - E_{DFT}^\circ(Cu) - E_{DFT}^\circ(Ga) - 2E_{DFT}^\circ(S), \tag{8}$$

where $E_{DFT}(CuGaS_2)$ is the DFT total energy of $CuGaS_2$ and $E_{DFT}^\circ(Cu)$, $E_{DFT}^\circ(Ga)$, and $E_{DFT}^\circ(S)$, are the DFT total energies of Cu, Ga, and S in their solid standard states. The B3LYP approximation does not provide accurate total energies for metallic Cu and Ga and so $E_{DFT}^\circ(Cu)$ and $E_{DFT}^\circ(Ga)$ are calculated from the relative stabilities of their compounds as

$$E_{DFT}^\circ(Cu) = \frac{1}{2}[E_{DFT}(Cu_2S) - E_{DFT}^\circ(S) - \Delta H_f^\circ(Cu_2S)], \tag{9}$$

$$E_{DFT}^\circ(Ga) = \frac{1}{2}[E_{DFT}(Ga_2S_3) - 3E_{DFT}^\circ(S) - \Delta H_f^\circ(Ga_2S_3)], \tag{10}$$

where $\Delta H_f^\circ(Cu_2S)$ and $\Delta H_f^\circ(Ga_2S_3)$ are the observed standard enthalpies of formation of $Cu_2S$ and $Ga_2S_3$ at 0 K.[28]

### E. Defect energetics

The formation of a defect can be considered in terms of an exchange between the host material and some atomic and electronic reservoirs. The Gibbs free energy of formation of a defect, $D$, in $CuGaS_2$ is given by[10,22]

$$\Delta G_D = E_{DFT}(D) - E_{DFT}(CuGaS_2) + \sum_i n_i \mu_i + q_D E_F, \tag{11}$$

where $E_{DFT}(D)$ and $E_{DFT}(CuGaS_2)$ are the DFT total energies of $CuGaS_2$ with and without the defect, $D$. The sign conven-

tion for $\Delta G_D$ is such that a negative value would lead to spontaneous formation of the defect unless it was kinetically hindered. The value of $E_{\mathrm{DFT}}(D)$, for charged defects, includes the correction terms discussed in Sec. II C. The third term represents the energy change due to the loss of $n_i$ atoms of element $i$ that occurs when the defect is formed (a negative value for $n_i$ denotes addition of atoms). The fourth term represents the energy change due to the exchange of electrons and holes with the carrier reservoirs; $q_D$ is the charge state of defect, $D$, and $E_F$ is the Fermi energy relative to the valence-band maximum (VBM) of the defect-free system. The Fermi energy is restricted to being above the VBM and below the conduction-band minimum (CBM).

### F. Defect concentration

In thermodynamic equilibrium, the concentration of defect $D$ is given by

$$c_D = N \exp\left[\frac{-\Delta G_D}{k_B T}\right], \tag{12}$$

where $N$ is the total number of atomic sites where defect $D$ can occur, $k_B$ is the Boltzmann constant, and $T$ is temperature. The overall system must be charge neutral,

$$\sum_D q_D c_D = 0. \tag{13}$$

The value of $\Delta G_D$ is a function of $E_F$, hence, Eqs. (12) and (13) can be solved self-consistently to obtain a value for $E_F$ and the equilibrium defect concentrations for each type of defect present. The carrier concentration of the system is then given by

$$\rho = \sum_D [n_D - q_D] c_D, \tag{14}$$

where $n_D$ is the change in the number of valence electrons in the system due to the formation of the neutral version of defect $D$. For example, $n_D=2$ for the defects $\mathrm{Ga_{Cu}}$, $\mathrm{Ga_{Cu}^{+}}$, and $\mathrm{Ga_{Cu}^{2+}}$ as a Ga atom has two more electrons in its valence shell than a Cu atom. This implies that $V_{\mathrm{S}}$ and $V_{\mathrm{S}}^{+}$ defects would each contribute two and one acceptors, respectively. A $V_{\mathrm{Se}}$ defect in $CuGaSe_2$ and $CuInSe_2$ does not, however, lead to the formation of two acceptors, instead the two electrons form a defect localized state that has an energy lower than the VBM.[29] Furthermore, an optical excitation of a $V_{\mathrm{Se}}^{2+}$ defect initiates the reaction $V_{\mathrm{Se}}^{2+} \rightarrow V_{\mathrm{Se}}^{0} + 2h$, that is two electrons become trapped in a localized defect state, releasing two holes to the valence band, similarly a $V_{\mathrm{Se}}^{+}$ defect releases one hole to the valence band. This mechanism is referred to as persistent hole photoconductivity ($p$-type PPC).[29] Analysis of the electronic structure of the analogous $V_{\mathrm{S}}^{+/2+}$ defects in $CuGaS_2$ shows that they also lead to $p$-type PPC behavior.

TABLE II. The calculated and observed lattice constants ($a$ and $c$) and anion displacement ($u$) for $CuGaS_2$.

| | $a$ (Å) | $c$ (Å) | $a/c$ | $u$ |
|---|---|---|---|---|
| Theory | 5.51 | 10.74 | 1.95 | 0.2592 |
| Observed[a] | 5.35 | 10.47 | 1.96 | 0.2539 |

[a]Reference 30.

## III. RESULTS AND DISCUSSION

### A. Bulk $CuGaS_2$

The computed and experimental lattice parameters and the anion displacement for $CuGaS_2$ are given in Table II. The lattice parameters are overestimated by around 2–3 %. This modest overestimation is typical for a hybrid exchange functional. The calculated band structure and density of states for $CuGaS_2$ are shown in Fig. 3. The calculated band gap is 2.12 eV at the Γ point, which is in reasonable agreement with the experimentally observed value of 2.43 eV.[32] The density of states between −5 and 0 eV is primarily due to hybridized Cu $d$ and S $p$ states. There is a $p$-$d$ repulsion gap between −3.2 and −2.0 eV which separates the bonding $p$-$d$ states from the antibonding $p$-$d$ states.

### B. Phase stability

The calculated values of $\Delta G$ for $CuGaS_2$ and the four binary phases considered are given in Table III. The definitions of $E_{\mathrm{DFT}}^{\circ}(\mathrm{Cu})$ and $E_{\mathrm{DFT}}^{\circ}(\mathrm{Ga})$ [Eqs. (9) and (10)] are such that the calculated values of $\Delta G_{\mathrm{Cu_2S}}$ and $\Delta G_{\mathrm{Ga_2S_3}}$ are equal to their observed values. The calculated values of $\Delta G_{\mathrm{CuS}}$ and

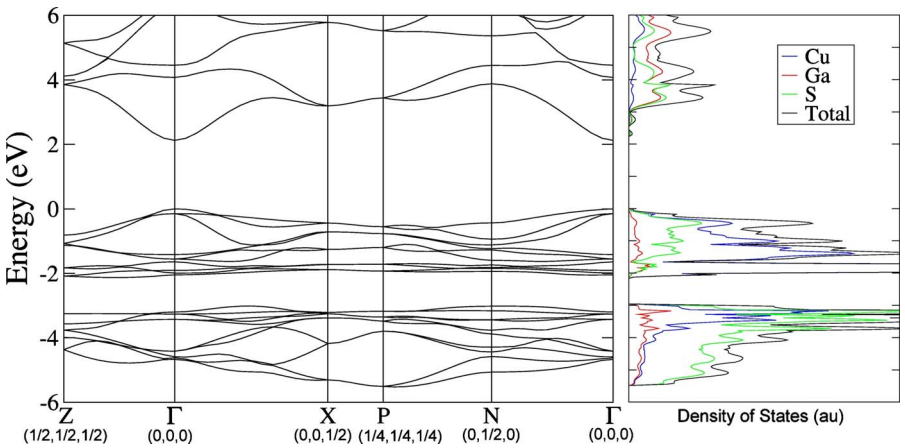


FIG. 3. (Color online) The calculated band structure and density of states for $CuGaS_2$. The Brillouin zones of the chalcopyrite lattice can be found elsewhere (Ref. 31).

TABLE III. Calculated Gibbs free energies of formation ($\Delta G$).

| Compound | $\Delta G$ (eV) |
|---|---|
| $CuGaS_2$ | −1.58 |
| $Cu_2S$ | −0.82 |
| CuS | −0.36 |
| $Ga_2S_3$ | −1.24 |
| GaS | −0.33 |

$\Delta G_{GaS}$ are, respectively, 0.29 eV and 0.19 eV greater than their observed values.[28] This overestimation has occurred, in part, because the basis sets used in the calculations have been optimized for $Cu^{1+}$, $Ga^{3+}$, and $S^{2-}$ ions. It is expected, therefore, that $\Delta G_{CuGaS_2}$ has been calculated more accurately than $\Delta G_{CuS}$ and $\Delta G_{GaS}$.

The stability region for $CuGaS_2$ as a function of $\Delta\mu_{Cu}$ and $\Delta\mu_{Ga}$ is shown in Fig. 4. It has been calculated from the observed values for $\Delta G_{CuS}$ and $\Delta G_{GaS}$ rather than the calculated values. For each point in the plane, the value of $\Delta\mu_S$ is determined from Eq. (5). The diagonal line which links the $\Delta\mu_{Cu}$ and $\Delta\mu_{Ga}$ axes represents $\Delta\mu_S=0$ eV. Moving in a direction perpendicular to this line, toward the origin, the value of $\Delta\mu_S$ decreases; at the origin $\Delta\mu_S=-0.79$ eV. The lines which represent $CuGaS_2$ in thermodynamic equilibrium with $CuGa_3S_5$ and $CuGa_5S_8$ are shown in the inset. These phases will be discussed in more detail in Sec. III D. The six vertices of the $CuGaS_2$ stability region have been labeled A-F. Properties of the material at the ABCDEF boundary will be discussed in the following sections.

The stability region for $CuGaS_2$ has been published previously.[33] In this previous paper, the relative differences between the calculated and observed values of $\Delta G$ for the binary phases are significantly larger than those calculated here. Figure 4 is, therefore, likely to provide a more accurate representation of the $CuGaS_2$ stability region.

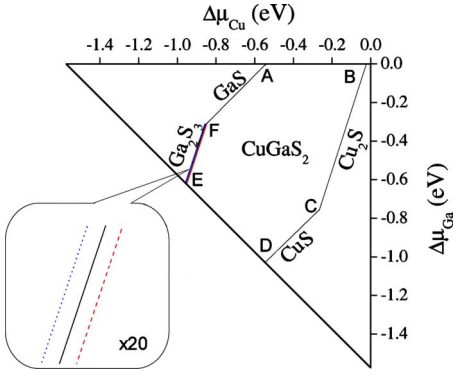


FIG. 4. (Color online) The stability region for $CuGaS_2$. The inset on the left is a 20 times magnification of the phase diagram showing where $CuGaS_2$ is in thermodynamic equilibrium with $CuGa_3S_5$ (the dotted blue line) and where $CuGaS_2$ is in equilibrium with $CuGa_5S_8$ (the dashed red line).

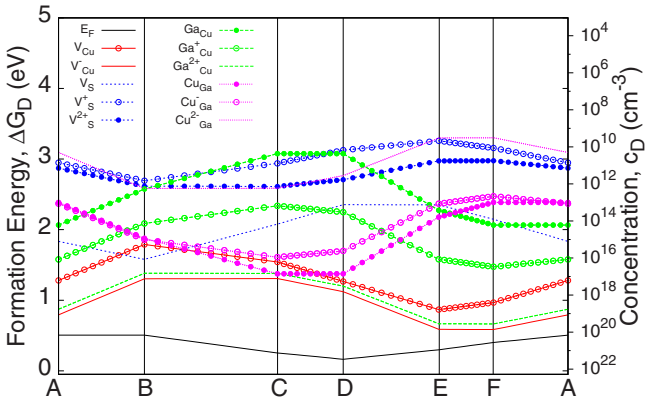


FIG. 5. (Color online) The formation energies and concentrations of the calculated defects along the boundary of the $CuGaS_2$ stability region (Fig. 4). The concentrations of $V_S$, $V_S^+$, and $V_S^{2+}$ are actually twice as large as those shown (as there are twice as many S atoms than Cu or Ga atoms in $CuGaS_2$). The lines which are represented by unfilled (filled) circles represent defects that contribute one (two) electron(s) or hole(s) toward the overall carrier concentration.

### C. Defect energies

The concentration of each defect at the ABCDEF boundary of the $CuGaS_2$ stability region was calculated using Eq. (12). A temperature of 1323 K was assumed as this is a typical temperature at which $CuGaS_2$ is produced by melt growth from its constituent elements.[34] The value of $E_F$ was determined self-consistently according to Eqs. (12) and (13). The calculated defect formation energies and $E_F$ are displayed in Fig. 5 (defects with very high formation energies have been omitted). The corresponding defect concentrations are also shown in this figure. The calculated defect formation energies, at $E_F=0$ and $\Delta\mu_i=0$ ($i$=Cu, Ga, and S), are given in Table IV.

The dominant intrinsic defects are $V_{Cu}^-$ and $Ga_{Cu}^{2+}$ defects which do not contribute toward the overall charge-carrier concentration. The resultant carrier concentration is predominately due to $V_{Cu}$ and $Cu_{Ga}$ defects. Close to point B, there are a large number of $V_S$ defects. This type of defect does

TABLE IV. Calculated defect formation energies, $\Delta G_D$, for intrinsic defects in $CuGaS_2$. Energies are quoted at $E_F=0$ and $\Delta\mu_i=0$ ($i$=Cu, Ga, and S).

| Vacancies | $\Delta G_D$ (eV) | Substitutions | $\Delta G_D$ (eV) |
|---|---|---|---|
| $V_{Cu}$ | 1.82 | $Ga_{Cu}$ | 2.60 |
| $V_{Cu}^-$ | 1.83 | $Ga_{Cu}^+$ | 1.61 |
| $V_{Ga}$ | 4.52 | $Ga_{Cu}^{2+}$ | 0.40 |
| $V_{Ga}^-$ | 4.69 | $Cu_{Ga}$ | 1.85 |
| $V_{Ga}^{2-}$ | 5.58 | $Cu_{Ga}^-$ | 2.34 |
| $V_{Ga}^{3-}$ | 7.14 | $Cu_{Ga}^{2-}$ | 3.57 |
| $V_S$ | 2.35 | | |
| $V_S^+$ | 2.96 | | |
| $V_S^{2+}$ | 2.38 | | |

not, however, contribute two electrons to the carrier concentration as the electrons form a delocalized state beneath the VBM (see Sec. II F). The $V_{Cu}$ and $Cu_{Ga}$ defects contribute one and two holes, respectively, to the system resulting in it being *p*-type doped. Along the ABCDEF boundary, the total carrier concentration varies between $4\times10^{15}$ and $6\times10^{18}$ $cm^{-3}$ at 1323 K. Hall measurements suggest that the material has a carrier concentration of around $10^{17}$ $cm^{-3}$ at room temperature, although it can vary quite substantially depending on the synthesis methods used.[34] Yu *et al.* measured the carrier concentration as a function of temperature over the range 110–400 K and fitted an analytical model to their data.[34] Assuming their model is valid at 1323 K then it is predicted that the carrier concentration increases by a factor of between 2 and 10 when the temperature is increased from 300 to 1323 K. The predicted carrier concentrations calculated at 1323 K are in good agreement with the experimental values extrapolated to this temperature.

### D. Compound defects and ordered defect compounds

It has previously been shown, for $CuGaSe_2$ and $CuInSe_2$, that the compound defect $2V_{Cu}^{-}+III_{Cu}^{2+}$ is energetically more favorable than the three isolated defects.[10] The formation energy of the analogous $2V_{Cu}^{-}+Ga_{Cu}^{2+}$ defect in $CuGaS_2$ is 1.57 eV lower than the combined energy of the three isolated defects.

The ordering of these compound defects leads to the formation of phases such as $CuGa_5S_8$ and $CuGa_3S_5$. These phases are referred to as ordered defect compounds (ODCs). Geometry optimization of $CuGa_5S_8$ and $CuGa_3S_5$ leads to a reduction in their equivalent cell volumes compared to $CuGaS_2$. The cell volume is reduced by 3.4% for $CuGa_5S_8$ and 2.6% for $CuGa_3S_5$. Analysis of the band structures of these ODC phases shows that the repulsion between the bonding and antibonding Cu *p* and S *d* states, seen in $CuGaS_2$ at around −3 eV, is much reduced, leading to a lowering of the VBMs of these phases compared to the VBM in $CuGaS_2$. The increased Ga content of $CuGa_5S_8$ and $CuGa_3S_5$ leads to a widening of their CBMs, and consequently, at their Γ points their CBMs are lower compared to the CBM of $CuGaS_2$. The lowering of the CBMs is greater than the lowering of the VBMs leading to an overall decrease in the band gaps of 7.5% and 9.4% for $CuGa_5S_8$ and $CuGa_3S_5$, respectively, compared to the band gap of $CuGaS_2$.

The stability regions for $CuGa_5S_8$ and $CuGa_3S_5$ are shown in Fig. 6. In both cases, the stability region is relatively small. In particular, the range of allowed $\Delta\mu_{Cu}$ values is very small. This suggests that the formation of these phases during the synthesis of $CuGaS_2$ is unlikely to occur under most experimental conditions. ODC phases have, however, been synthesized but shown only to occur in a small region of phase space.[35,36] Kokta *et al.*[35] reported that they had observed $CuGa_5S_8$ while Tsubaki *et al.*[36] speculated that they had synthesized $CuGa_3S_5$.

### E. Extrinsic defects and *n*-type doping

In this section, the possibility of *n*-type doping $CuGaS_2$ through the incorporation of extrinsic defects is investigated.

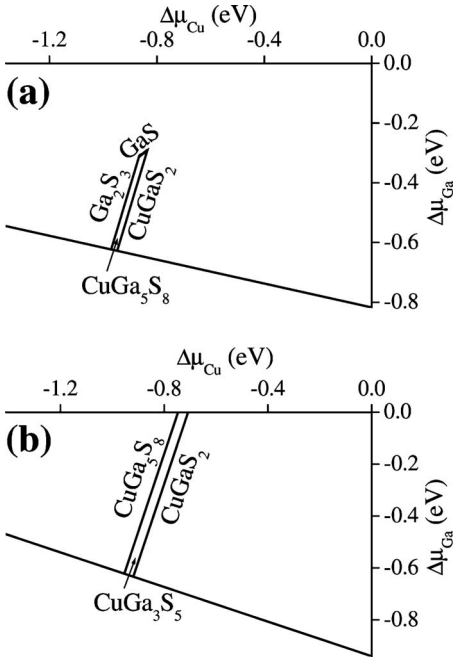


FIG. 6. The stability regions for (a) $CuGa_5S_8$ and (b) $CuGa_3S_5$. The values for $\Delta\mu_S$ are obtained from the requirement that the sum of the three chemical potentials must equal the energy of formation of the compound defects. The minimum allowed values of $\Delta\mu_S$ for $CuGa_5S_8$ and $CuGa_3S_5$ are −0.51 eV and −0.56 eV, respectively (compared to −0.79 eV for $CuGaS_2$). Only three phases are shown in each diagram, the one of primary interest and the two phases that form a boundary with this phase.

To *n*-type dope $CuGaS_2$ through the incorporation of group II atoms, it must be energetically favorable to form neutral $II_{Cu}$ defects rather than neutral $II_{Ga}$ defects. Formation energies for $II_{Cu}$ and $II_{Ga}$ defects (II=Mg, Zn, and Cd) are given in Table V at $E_F=0$ and $\Delta\mu_i=0$ ($i$=Cu, Ga, and S). When $\Delta\mu_{Cu}=\Delta\mu_{Ga}$, the neutral $II_{Ga}$ defect is energetically more stable than the neutral $II_{Cu}$ defect. A group II element will only preferentially replace Cu rather than Ga when

TABLE V. Formation energies, $\Delta G_D$, at $E_F=0$ and $\Delta\mu_i=0$ ($i$=Cu, Ga, and S) for $II_{Cu}$ and $II_{Ga}$ defects in $CuGaS_2$.

| Defect | $\Delta G_D$ (eV) |
|---|---|
| $Mg_{Cu}$ | −0.63 |
| $Mg_{Cu}^{+}$ | −3.00 |
| $Zn_{Cu}$ | 0.71 |
| $Zn_{Cu}^{+}$ | −1.68 |
| $Cd_{Cu}$ | 1.31 |
| $Cd_{Cu}^{+}$ | −1.23 |
| $Mg_{Ga}$ | −1.67 |
| $Mg_{Ga}^{-}$ | −1.46 |
| $Zn_{Ga}$ | −0.38 |
| $Zn_{Ga}^{-}$ | −0.10 |
| $Cd_{Ga}$ | 0.38 |
| $Cd_{Ga}^{-}$ | 0.82 |

TABLE VI. Formation energies, $\Delta G$, at $E_F=0$ and $\Delta\mu_i=0$ ($i$ =Cu, Ga, and S) for $IV_{Ga}$ defects in $CuGaS_2$.

| Defect | $\Delta G$ (eV) |
|---|---|
| $Ge_{Ga}$ | 1.10 |
| $Ge_{Ga}^{+}$ | −0.45 |
| $Sn_{Ga}$ | 1.04 |
| $Sn_{Ga}^{+}$ | −0.98 |

$$\Delta\mu_{Ga}-\Delta\mu_{cu}>\Delta G_{II_{Cu}}-\Delta G_{II_{Ga}}. \quad (15)$$

The minimum value of $\Delta G_{II_{Cu}}-\Delta G_{II_{Ga}}$ is 0.93 eV, when II =Cd. The maximum value of $\Delta\mu_{Ga}-\Delta\mu_{Cu}$ consistent with the stability of bulk $CuGaS_2$ is 0.54 eV (line FA in Fig. 4). It is, therefore, predicted that it is not possible to $n$-type dope $CuGaS_2$ by the introduction of Mg, Zn, or Cd.

Another possibility might be to $n$-type dope $CuGaS_2$ by introducing $IV_{Ga}$ defects (IV=Ge and Sn). The formation energies of these defects are given in Table VI. The electronic structure of $CuGaS_2$ with $Ge_{Ga}$ and $Sn_{Ga}$ defects is shown in Fig. 7. The defects cause the formation of a half-filled intermediate band. In the case of the $Ge_{Ga}$ defect, this band is located 1.15 eV below the CB at the $\Gamma$ point while for the $Sn_{Ga}$ defect, it is located approximately 0.91 eV below the CB. The formation of the IB means that while the addition of a group IV element is unlikely to contribute toward the $n$-type behavior of $CuGaS_2$, it may, however, lead to an effective intermediate band absorber material.

An alternative method that may lead to $n$-type doping of the material is to introduce $VII_S$ defects (VII=Cl, Br, or I). The formation energies for these defects are given in Table VII. It is easier to incorporate Cl into the lattice than Br or I. This is to be expected as the ionic radius of S (1.84 Å) is a closer match to the ionic radius of Cl (1.81 Å) than to Br (1.96 Å) or I (2.20 Å).

To maximize Cl incorporation $\Delta\mu_S$ has to be minimized and, simultaneously, $\Delta\mu_{Cl}$ has to be maximized. The minimum value of $\Delta\mu_S$ within the phase stability region occurs at

TABLE VII. Formation energies, $\Delta G_D$, at $E_F=0$ and $\Delta\mu_i=0$ ($i$ =Cu, Ga, and S) for $VII_S$ defects in $CuGaS_2$.

| Defect | $\Delta G_D$ (eV) |
|---|---|
| $Cl_S$ | 1.30 |
| $Cl_S^{+}$ | −0.87 |
| $Br_S$ | 4.15 |
| $Br_S^{+}$ | 1.81 |
| $I_S$ | 7.41 |
| $I_S^{+}$ | 4.94 |

position B (Fig. 4) where $\Delta\mu_S=-0.78$ eV. Allowed values of $\Delta\mu_{Cl}$ are constrained by the condition that the competing phase, $GaCl_3$, does not become more stable than $CuGaS_2$. This implies that $3\Delta\mu_{Cl}+\Delta\mu_{Ga}\leq-4.15$ eV. At position B $\Delta\mu_{Ga}=0$ eV, hence, the maximum allowed value of $\Delta\mu_{Cl}$ is −1.38 eV. At $\Delta\mu_{Cl}=-1.38$ eV $E_F=1.03$ eV [$E_F$ is obtained using Eqs. (11)–(13)] and the material is $p$-type doped with a carrier concentration of $8\times10^{16}$ $cm^{-3}$. Comparing this to the intrinsic $p$-type doping of $2\times10^{15}$ $cm^{-3}$, it can be seen that the inclusion of Cl has actually increased the $p$-type doping. This is due to the stability of the $Cl_S^{+}$ defect. This defect increases the value of $E_F$, consequently the $p$-type defect $Cu_{Ga}^{-}$ becomes more stable. It is, hence, predicted that is not possible to $n$-type dope the system by introducing group VII elements.

## IV. CONCLUSIONS

The phase stability region of $CuGaS_2$ as a function of its chemical potentials, $\Delta\mu_{Cu}$, $\Delta\mu_{Ga}$, and $\Delta\mu_S$, has been calculated. It has been shown that the compound defect $2V_{Cu}^{-}+Ga_{Cu}^{2+}$ is stable with respect to the formation of the three isolated defects by 1.57 eV. The ordered defect compounds $CuGa_3S_5$ and $CuGa_5S_8$ are predicted to be stable in a small region of $\Delta\mu_i$ ($i$=Cu, Ga, and S) phase space.

It is predicted that the dominant intrinsic defects in $CuGaS_2$ are $V_{Cu}^{-}$ and $Ga_{Cu}^{2+}$ which do not contribute toward

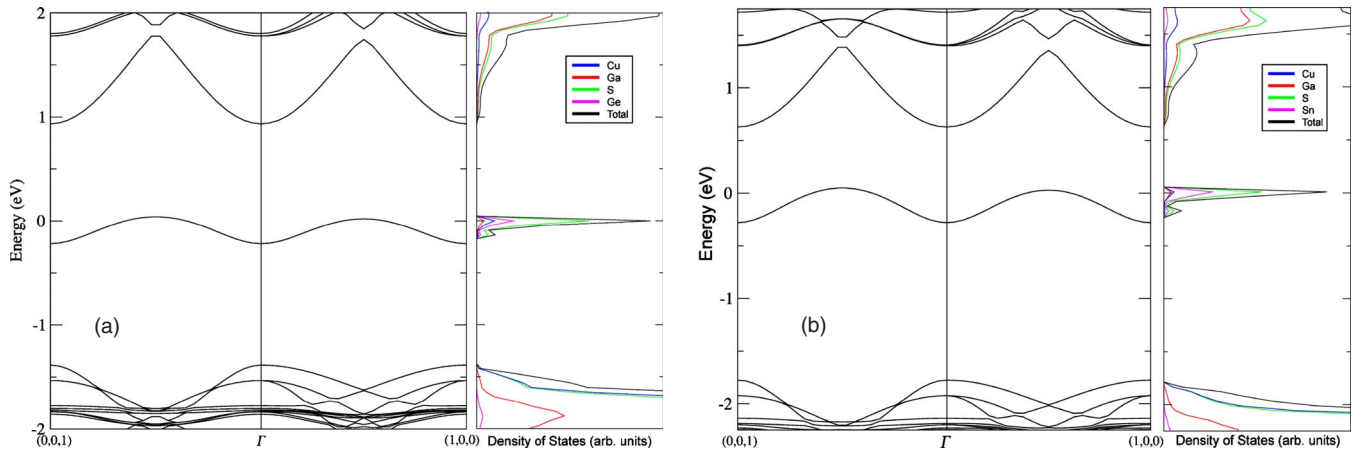


FIG. 7. (Color online) The calculated band structure and density of states for (a) $Ge_{Ga}$ defects and (b) $Sn_{Ga}$ defects in $CuGaS_2$.

the overall charge-carrier concentration. The carrier concentration is predominately due to $V_{Cu}$ and $Cu_{Ga}$ defects. These defects donate one and two holes, respectively, to $CuGaS_2$, hence the intrinsic material is always *p*-type doped at thermodynamic equilibrium. The calculated intrinsic charge-carrier concentration of around $10^{17}$ $cm^{-3}$ agrees very well with experimentally observed values.

Attempts to *n*-type dope $CuGaS_2$ through the addition of extrinsic defects consisting of group II, IV, and VII atoms failed. The most promising method of *n*-type doping was to incorporate $VII_S$ defects into the material. The $VII_S^+$ defects where, however, always significantly more stable than the $VII_S$ defects. This leads to an increase in the Fermi energy and consequent stabilization of the *p*-type $Cu_{Ga}^-$ defect. This difficulty in *n*-type doping $CuGaS_2$ may limit its effectiveness in photovoltaic devices. It was shown, however, that the incorporation of $IV_{Ga}$ defects (IV=Sn and Ge) results in the formation of a half-filled IB, suggesting that this type of defect in $CuGaS_2$ has potential for use in the design of an IB absorber material.

## ACKNOWLEDGMENTS

The calculations were performed in part on the STFC's SCARF and NW-Grid systems and in part the U.K.'s national high-performance computing service, HECToR, where computer time has been provided via our membership of the U.K.'s HPC Materials Chemistry Consortium and funded by EPSRC (portfolio Grant No. EP/F067496).

[1] W. Shockley and H. J. Queisser, J. Appl. Phys. **32**, 510 (1961).
[2] A. Luque and A. Marti, Phys. Rev. Lett. **78**, 5014 (1997).
[3] S. Tomić, T. S. Jones, and N. M. Harrison, Appl. Phys. Lett. **93**, 263105 (2008).
[4] A. Martí, D. F. Marrón, and A. Luque, J. Appl. Phys. **103**, 073706 (2008).
[5] P. Palacios, K. Sanchez, J. C. Conesa, J. J. Fernandez, and P. Wahnon, Thin Solid Films **515**, 6280 (2007).
[6] P. Palacios, I. Aguiler, P. Wahnon, and J. C. Conesa, J. Phys. Chem. C **112**, 9525 (2008).
[7] M. Bär, S. Nishiwaki, L. Weinhardt, S. Pookpanratana, O. Fuchs, M. Blum, W. Yang, J. D. Denlinger, W. N. Shafarman, and C. Heske, Appl. Phys. Lett. **93**, 244103 (2008).
[8] Y. J. Zhao, C. Persson, S. Lany, and A. Zunger, Appl. Phys. Lett. **85**, 5860 (2004).
[9] C. Persson, Y. J. Zhao, S. Lany, and A. Zunger, Phys. Rev. B **72**, 035211 (2005).
[10] S. B. Zhang, S. H. Wei, A. Zunger, and H. Katayama-Yoshida, Phys. Rev. B **57**, 9642 (1998).
[11] S. Wei, S. B. Zhang, and A. Zunger, Appl. Phys. Lett. **72**, 3199 (1998).
[12] R. Dovesi, V. R. Saunders, C. Roetti, R. Orlando, C. M. Zicovich-Wilson, F. Pascale, B. Civalleri, K. Doll, N. M. Harrison, I. J. Bush, P. D'Arco, and M. Llunell, *CRYSTAL 2006 Users's Manual* (University of Torino, Turin, Italy 2007).
[13] A. D. Becke, J. Chem. Phys. **98**, 1372 (1993).
[14] J. Muscat, A. Wander, and N. M. Harrison, Chem. Phys. Lett. **342**, 397 (2001).
[15] S. Tomić, B. Montanari, and N. M. Harrison, Physica E **40**, 2125 (2008).
[16] J. Heyd, J. E. Peralta, and G. E. Scuseria, J. Chem. Phys. **123**, 174101 (2005).
[17] A. Lichanot E. Apra and R. Dovesi, Phys. Status Solidi **177**, 157 (1993).
[18] T. Homann, U. Hotje, M. Binnewies, A. Borger, K. D. Becker, and T. Bredow, Solid State Sci. **8**, 44 (2006).
[19] K. Doll and N. M. Harrison, Chem. Phys. Lett. **317**, 282 (2000).
[20] See supplementary material at http://link.aps.org/supplemental/10.1103/PhysRevB.81.205214 for details of basis sets.
[21] P. Ewald, Ann. Phys. **369**, 253 (1921).
[22] C. G. Van de Walle and J. Neugebauer, J. Appl. Phys. **95**, 3851 (2004).
[23] G. Makov and M. C. Payne, Phys. Rev. B **51**, 4014 (1995).
[24] C. Darrigan, M. Rérat, G. Mallia, and R. Dovesi, J. Comput. Chem. **24**, 1305 (2003).
[25] C. W. M. Castleton, A. Hoglund, and S. Mirbt, Modell. Simul. Mater. Sci. Eng. **17**, 084003 (2009).
[26] X. G. Wang, W. Weiss, S. K. Shaikhutdinov, M. Ritter, M. Petersen, F. Wagner, R. Schlogl, and M. Scheffler, Phys. Rev. Lett. **81**, 1038 (1998).
[27] K. Reuter and M. Scheffler, Phys. Rev. B **65**, 035406 (2001).
[28] M. W. Chase, C. A. Davies, J. R. Downey, D. J. Frurip, R. A. McDonald, and A. N. Syverud, J. Phys. Chem. Ref. Data **14**, 927 (1985).
[29] S. Lany and A. Zunger, Phys. Rev. B **72**, 035215 (2005).
[30] S. C. Abrahams and J. L. Bernstein, J. Chem. Phys. **59**, 5415 (1973).
[31] O. Madelung, *Seminconductors: Data Handbook* (Springer, New York, 2003).
[32] J. L. Shay and J. H. Wernick, *Ternary Chalcopyrite Semiconductors: Growth, Electronic Properties and Applications*, (Pergamon Press, Oxford, 1974).
[33] Y. J. Zhao and A. Zunger, Phys. Rev. B **69**, 075208 (2004).
[34] P. W. Yu, D. L. Downing, and Y. S. Park, J. Appl. Phys. **45**, 5283 (1974).
[35] M. Kokta, J. R. Carruthers, M. Grasso, H. M. Kasper, and B. Tell, J. Elecron. Mater. **5**, 69 (1976).
[36] K. Tsubaki and K. Sugiyama, J. Electron. Mater. **12**, 43 (1983).